Exploiting Deep Learning in the Performance Evaluation of EH-Based Coordinated Direct and Relay Transmission System With Cognitive NOMA

Alok Kumar Shukla, *Graduate Student Member, IEEE*, Kajal Yadav, *Graduate Student Member, IEEE*, Prabhat Kumar Upadhyay, *Senior Member, IEEE*, and Jules M. Moualeu, *Senior Member, IEEE*

***Abstract*— This letter investigates an energy harvesting (EH)-assisted coordinated direct and relay transmission in an overlay cognitive non-orthogonal multiple access (NOMA) system assuming perfect and imperfect successive interference cancellation. Specifically, we derive analytical expressions of the outage probability (OP) which include an infinite series, system throughput, and energy efficiency. Moreover, an asymptotic analysis of the OP in the high signal-to-noise ratio is carried out. Closed-form expressions of the exact OP and the ergodic sum capacity (ESC) are intractable owing to the complexity of the proposed scheme. To tackle this problem, we propose a deep learning (DL) framework to predict both the OP and ESC performances. The predicted results through the DL framework are shown to be consistent with the numerical results.**

***Index Terms*— Cognitive radio, coordinated direct and relay transmission, deep learning, energy harvesting, NOMA, SWIPT.**

I. Introduction

THE integration of device-to-device communication and the internet of things (IoT) into contemporary communication systems has demonstrated the necessity for efficient spectrum and energy utilisation. In this regard, non-orthogonal multiple access (NOMA) and simultaneous wireless information and power transmission (SWIPT) are envisioned as promising technologies for improving the spectral efficiency (SE) and energy efficiency (EE) in future wireless systems [1]. In the former, the transmitter uses superposition coding while the receiver uses successive interference cancellation (SIC) to accommodate multiple users over the same code, frequency, and time resources that yields SE improvement. In the latter, both energy and information are retrieved simultaneously from the radio frequency (RF) signal being delivered at the energy-constrained receiver node.

To further enhance the SE and network coverage, cooperative relaying with NOMA was incorporated in [2] where users with stronger channels act as relays to communicate with users with weaker channels. The authors in [3] examined the full/half-duplex relaying for cooperative NOMA to analyze the outage performance, diversity order and ergodic rate. Moreover, a NOMA-based coordinated direct and relay transmission (CDRT) technique has been proposed in [4] and subsequently explored in [5], [6], [7], and [8]. Specifically, the authors in [5] investigated a device-to-device aided NOMA-based CDRT network which has shown to outperform the conventional CDRT network in terms of ergodic sum capacity (ESC) and sum throughput. The system performance of an IoT-based CDRT with NOMA-assisted network was evaluated in [6]. In [7], the authors examined the performance of a CDRT-NOMA system by considering direct links with far and near users along with amplify-and-forward (AF) and decode-and-forward (DF) relaying protocols. A deep neural network (DNN) was designed in [8] to evaluate the performance of underlay cognitive NOMA-based CDRT networks. On another front, a series of works have investigated SWIPT-assisted NOMA networks using a time-switching (TS) based energy harvesting (EH) relaying protocol [9], [10]. A particle swarm optimization algorithm was proposed to optimize the TS and power allocation factors for a SWIPT-assisted NOMA network in [9]. In [10], a SWIPT assisted NOMA-based CDRT network was investigated to improve the outage performance by optimizing the TS factor.

Most of the above-mentioned works using the NOMA-based CDRT scheme have employed cooperative relaying to communicate with its weak users assuming perfect SIC (pSIC). However, pSIC is not realistic in practical systems; it is therefore crucial to investigate the limitations that the non-idealities of SIC may pose on the proposed scheme. More recently, the adoption of the underlay [8] or overlay [10] cognitive radio (CR) technology in NOMA-based CDRT networks has shown significant improvement in the network performance. However, the stringent restrictions imposed on the transmit power in the underlay CR make its overlay counterpart more attractive. Yet, its incorporation in the EH-aided NOMA-based CDRT networks remains vastly unexplored. Inspired by the preceding discussion, we propose a novel system that integrates a power-splitting (PS)-based EH receiver architecture in an overlay CR NOMA-based CDRT network. Although the work in [10] studies an overlay CR NOMA-based CDRT scheme, it does not investigate the performance of the ESC and no data-driven approach on the performance evaluation is provided. In this letter, we derive novel analytical expressions of the outage probability (OP), system throughput, and EE under both the pSIC and imperfect SIC (ipSIC) cases. Moreover, we obtain asymptotic OP expressions at high signal-to-noise ratio (SNR) to provide useful insights. However, the derivation of the closed-form expression of the OP is intractable, let alone the ergodic capacity (EC)/ESC. This is due to the high complexity and variability of the proposed system model as characterized by emerging communications system requirements. To address these limitations, we propose a data-driven approach through deep learning (DL) to estimate the exact ergodic capacity (EC)/ESC along with OP with a high accuracy and low latency.

II. System Model

As shown in Fig. 1, we propose an EH-based CDRT system with an overlay cognitive NOMA scheme, wherein the primary network consists of a source node S, a near-user D_1 and a far-user D_2, while the secondary network consists of an energy-constrained IoT-transmitter node I (which acts as a PS-based EH DF relay) and an IoT-receiver node R. All the nodes are assumed to be equipped with a single antenna. Here, node S directly communicates with node D_1. It is assumed that the direct link between node S and D_2 is absent [6]. Thus, S seeks relay cooperation from node I

Manuscript received 2 January 2023; revised 11 February 2023; accepted 14 March 2023. Date of publication 17 March 2023; date of current version 12 June 2023. The work of K. Yadav is supported in part by the Prime Minister's Research Fellow (PMRF) scheme. The work of P. K. Upadhyay is supported in part by the Visvesvaraya Young Faculty Research Fellow (YFRF) Scheme of MeitY, Government of India. The research of J. M. Moualeu is supported in part by the NRF of South Africa under the BRICS Multilateral R&D Project (Grant No. 116018). The associate editor coordinating the review of this letter and approving it for publication was M. Wen. *(Corresponding author: Jules M. Moualeu.)*

Alok Kumar Shukla, Kajal Yadav, and Prabhat Kumar Upadhyay are with the Department of Electrical Engineering, IIT Indore, Indore, Madhya Pradesh 453552, India (e-mail: phd1901102019@iiti.ac.in; mtphd2206102001@iiti.ac.in; pkupadhyay@iiti.ac.in).

Jules M. Moualeu is with the School of Electrical and Information Engineering, University of the Witwatersrand, Johannesburg 2000, South Africa (e-mail: jules.moualeu@wits.ac.za).

Digital Object Identifier 10.1109/LCOMM.2023.3258665

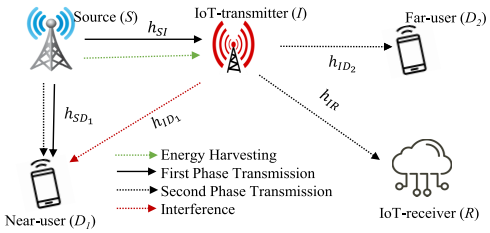

Fig. 1. System model.

to communicate with its far-user D_2. As the IoT-transmitter node I is energy-constrained, it first harvests energy from the received RF signal from node S and then splits the corresponding received power to relay the primary signal and to transmit its own signal. The channel coefficient and distance between any two nodes j and k are represented by h_{jk} and d_{jk}, respectively, with $j \in (S, I)$, $k \in (D_1, I, D_2, R)$, and $j \neq k$. It is assumed that all the channels experience Rayleigh fading except the channel h_{SD_1} which follows a Rician distribution due to the viability of a line-of-sight link. Therefore, $|h_{jk}|^2$, for $j \in (S, I)$, $k \in (I, D_2, R)$, $j \neq k$, is an exponential random variable (RV) with mean $\lambda_{jk} = d_{jk}^{-\nu}$, where ν denotes the path-loss exponent and $|h_{SD_1}|^2$ is a non-central chi-square distributed RV with mean $\lambda_{SD_1} = d_{SD_1}^{-\nu}$. Under statistical channel state information, it is assumed that the average channel powers associated with links $j \to k$, $j \in (S, I)$, $k \in (I, D_2, R)$, $j \neq k$ are ordered as $\lambda_{SI} < \lambda_{SD_1}$ and $\lambda_{ID_1} < \lambda_{IR} < \lambda_{ID_2}$, without loss of generality [11].[1] The probability density function (PDF) and cumulative distribution function (CDF) of $W \triangleq |h_{SD_1}|^2$ are given, respectively, by $f_W(w) = \phi e^{-(\phi w + K)} I_0\left(2\sqrt{\phi K w}\right)$ and $F_W(w) = 1 - Q_1\left(\sqrt{2K}, \sqrt{2\phi w}\right)$, where $\phi = \frac{(1+K)}{\lambda_{SD_1}}$, K is the Rician K-factor, $I_0(\cdot)$ is the modified Bessel function of the first kind [12, eq. 8.447], and $Q_1(\cdot, \cdot)$ is the Marcum-Q function [13, eq. 4.10]. All the links are inflicted by additive white Gaussian noise (AWGN) with mean zero and variance σ^2. The overall communication occurs in two phases over a transmission block of duration T as described in the sequel.

A. First Phase Transmission

For the first phase transmission of duration $T/2$ (denoted by t_1), source node S broadcasts the superimposed signal $X_S = \sum_{m=1}^{2} \sqrt{\alpha_m P_s} x_m$ towards D_1 and node I. Here, P_s denotes the source's transmit power, x_m is the intended signal for D_m, α_m is the power allocation factor (PAF), $m \in (1, 2)$, with $\sum_{m=1}^{2} \alpha_m = 1$ and $\alpha_2 > \alpha_1$. Thus, the signal received at node k, $k \in (D_1, I)$, can be given by $y_{Sk}^{t_1} = h_{Sk} X_S + n_{Sk}$, where n_{Sk} is the AWGN variable. Following the NOMA principle, D_1 first decodes signal x_2 assuming x_1 as noise, and then applies SIC to decode signal x_1. Thus, the signal-to-interference-plus-noise ratios (SINRs) at D_1 to decode x_2 and x_1, respectively, are given by

$$\gamma_{S \to D_1}^{x_2, t_1} = \frac{\alpha_2 \rho_s |h_{SD_1}|^2}{\alpha_1 \rho_s |h_{SD_1}|^2 + 1}, \tag{1}$$

$$\gamma_{S \to D_1}^{x_1, t_1} = \frac{\alpha_1 \rho_s |h_{SD_1}|^2}{\psi_1 \alpha_2 \rho_s |h_{SD_1}|^2 + 1}, \tag{2}$$

where $\rho_s = P_s/\sigma^2$ is the transmit SNR, ψ_1 $(0 \leq \psi_1 \leq 1)$ is the residual interference parameter and $\psi_1 = 0$ denotes the pSIC case. However, the received signal at I is bifurcated as $\sqrt{\beta} y_{SI}^{t_1}$ for EH and $\sqrt{(1-\beta)} y_{SI}^{t_1}$ for information transmission, where $0 \leq \beta \leq 1$ represents the PS factor. The received signal for EH at node I can be expressed as

$$\sqrt{\beta} y_{SI}^{t_1} = \sqrt{\beta} h_{SI} X_s + \sqrt{\beta} n_{SI}. \tag{3}$$

[1]The decoding method adopted in this work is based on the average power λ_{jk}, i.e., on the distance. Although, this is not a standard approach, it may have some practical feasibility [11].

From (3), the harvested energy at node I can be given by

$$E_h = \beta\mu \left(P_s \alpha_1 + P_s \alpha_2\right) |h_{SI}|^2 T/2 = \beta\mu P_s |h_{SI}|^2 T/2, \tag{4}$$

where μ $(0 < \mu \leq 1)$ indicates the energy conversion efficiency, and the noise statistic is ignored [14]. Thus, the transmit power of node I for the remaining $T/2$ period can be given as $P_r = \frac{E_h}{T/2} = \beta\mu |h_{SI}|^2 P_s$ while the received base-band signal at node R is given by

$$\sqrt{(1-\beta)} y_{SI}^{t_1} = \sqrt{(1-\beta)} h_{SI} \left(\sum_{m=1}^{2} \sqrt{\alpha_m P_s} x_m \right) + N_{SI}, \tag{5}$$

where $N_{SI} = \sqrt{(1-\beta)} n_{SI} + n_{RF}$, and n_{RF} is the sampled AWGN due to RF to base-band signal conversion. Thus, the SINR at I to decode x_2 can be expressed as

$$\gamma_{S \to I}^{x_2, t_1} = \frac{\alpha_2 (1-\beta) \rho_s |h_{SI}|^2}{\alpha_1 (1-\beta) \rho_s |h_{SI}|^2 + 1}. \tag{6}$$

B. Second Phase Transmission

In the next $T/2$ time period (denoted by t_2), upon successful decoding of x_2, node I combines its own signal x_i with x_2 as $X_I = \sqrt{\alpha_3 P_r} x_i + \sqrt{\alpha_4 P_r} x_2$, where x_i and x_2 are intended signals for R and D_2 respectively, α_3 and α_4 are PAFs. Here, we assume that $d_{IR} > d_{ID_2}$, yielding $\alpha_3 > \alpha_4$ and $\alpha_3 + \alpha_4 = 1$. Thus, the signal received at node p, $p \in (R, D_2)$, can be written as $y_{Ip}^{t_2} = h_{Ip} X_I + n_{Ip}$. Herein, signal x_i is directly decoded at node R and SIC is conducted at D_2 to decode x_2. Thus, the received SINR to decode x_i at node R can be given as

$$\gamma_{I \to R}^{x_i, t_2} = \frac{\alpha_3 \beta\mu \rho_s |h_{SI}|^2 |h_{IR}|^2}{\alpha_4 \beta\mu \rho_s |h_{SI}|^2 |h_{IR}|^2 + 1}. \tag{7}$$

After applying the SIC, the end-to-end SINRs to decode x_i and x_2 at D_2 can be expressed, respectively, as

$$\gamma_{I \to D_2}^{x_i, t_2} = \frac{\alpha_3 \beta\mu \rho_s |h_{SI}|^2 |h_{ID_2}|^2}{\alpha_4 \beta\mu \rho_s |h_{SI}|^2 |h_{ID_2}|^2 + 1}, \tag{8}$$

$$\gamma_{I \to D_2}^{x_2, t_2} = \frac{\alpha_4 \beta\mu \rho_s |h_{SI}|^2 |h_{ID_2}|^2}{\psi_2 \alpha_3 \beta\mu \rho_s |h_{SI}|^2 |h_{ID_2}|^2 + 1}, \tag{9}$$

where ψ_2 $(0 \leq \psi_2 \leq 1)$ is the residual interference parameter.

In order to maximize spectrum utilization, source S simultaneously transmits the new signal $\hat{x}_1$ to D_1 with transmit power $\sqrt{\alpha_1^* P_s}$, for $\alpha_1^* \in (0, 1)$, during the second phase. However, during the second phase transmission, D_1 experiences some interference from node I, which can be estimated and partially eliminated by using the side information of x_2 that is obtained during the SIC process in the first phase transmission. Therefore, the signal received during the second phase at D_1 can be given as $y_{SD_1}^{t2} = \sqrt{\alpha_1^* P_s} h_{SD_1} \hat{x}_1 + h_{ID_1} X_I + n_{SD_1}$, and the corresponding SINR, after partial interference cancellation can be expressed as

$$\gamma_{S \to D_1}^{\hat{x}_1, t_2} = \frac{\alpha_1^* \rho_s |h_{SD_1}|^2}{\alpha_3 \mu\beta \rho_s |h_{SI}|^2 |h_{ID_1}|^2 + 1}. \tag{10}$$

III. Performance Analysis

Considering the target data rates r_{d_1}, r_{d_2}, and r_r for D_1, D_2, and R, respectively, we execute the performance analysis of the proposed EH-based CDRT-NOMA system as follows.

A. OP Analysis

1) Near-User D_1: In the first phase, D_1 is said to be in outage if it is unable to decode either of the symbols x_1 or x_2. Hence, its OP expression is given by

$$P_{D_1}^{\text{out}, t_1} = 1 - \Pr\left[\gamma_{S \to D_1}^{x_2, t_1} > \gamma_{D_2}^{\text{th}}, \gamma_{S \to D_1}^{x_1, t_1} > \gamma_{D_1}^{\text{th}}\right], \tag{11}$$

where $\gamma_{D_1}^{\text{th}} = 2^{2r_{d_1}} - 1$ and $\gamma_{D_2}^{\text{th}} = 2^{2r_{d_2}} - 1$. By substituting the involved SINRs from (1) and (2) in (11), and performing some algebraic manipulations, $P_{D_1}^{\text{out},t_1}$ can be expressed as

$$P_{D_1}^{\text{out},t_1} = 1 - \Pr\left[|h_{SD_1}|^2 > \frac{\max\{\mathcal{A}_1, \mathcal{A}_2\}}{\rho_s}\right], \tag{12}$$

where $\mathcal{A}_1 = \frac{\gamma_{D_2}^{\text{th}}}{\alpha_2 - \alpha_1 \gamma_{D_2}^{\text{th}}}$ and $\mathcal{A}_2 = \frac{\gamma_{D_1}^{\text{th}}}{\alpha_1 - \psi_1 \alpha_2 \gamma_{D_1}^{\text{th}}}$. Under the conditions $\frac{\alpha_2}{\alpha_1} > \gamma_{D_2}^{\text{th}}$ and $\frac{\alpha_1}{\psi_1 \alpha_2} > \gamma_{D_1}^{\text{th}}$, (12) can be further re-expressed and evaluated as

$$P_{D_1}^{\text{out},t_1} = \Pr[W \le \Delta_1/\rho_s] = 1 - Q_1\left(\sqrt{2K}, \sqrt{2\phi\Delta_1/\rho_s}\right), \tag{13}$$

where $\Delta_1 \triangleq \max\{\mathcal{A}_1, \mathcal{A}_2\}$. At high SNR ($\rho_s \to \infty$), the asymptotic expression for $P_{D_1}^{\text{out},t_1}$ can be obtained by making use of [15, eq. 9.6.7] and the following approximation $e^{-x} \simeq 1 - x$ for small x in (13). It can be given by

$$P_{D_1,asy}^{\text{out},t_1} = \phi e^{-K} \Delta_1/\rho_s. \tag{14}$$

In the second phase transmission, the OP for D_1 is given by

$$P_{D_1}^{\text{out},t_2} = \Pr\left[\gamma_{S\to D_1}^{\hat{x}_1,t_2} < \gamma_{D_1}^{\text{th}}\right]. \tag{15}$$

By substituting (10) in (15), and after doing some mathematical re-arrangement, $P_{D_1}^{\text{out},t_2}$ can be written as

$$P_{D_1}^{\text{out},t_2} = \Pr[W < \mathcal{B}_1 XV + \mathcal{B}_2], \tag{16}$$

with $V \triangleq |h_{ID_1}|^2$, $X \triangleq |h_{SI}|^2$, $\mathcal{B}_1 = \frac{\gamma_{D_1}^{\text{th}} \alpha_3 \beta\mu}{\alpha_1^*}$ and $\mathcal{B}_2 = \frac{\gamma_{D_1}^{\text{th}}}{\alpha_1^* \rho_s}$.

Theorem 1: The expression of $P_{D_1}^{\text{out},t_2}$ in (16) can be given by

$$P_{D_1}^{\text{out},t_2} = 1 - \sum_{l=0}^{\infty}\sum_{m=0}^{l}\sum_{n=0}^{m}\binom{m}{n}\frac{\mathcal{B}_2^{m-n}K^l n!\mathcal{B}_1^n\phi^m e^{-K}}{l!m!\lambda_{SI}\lambda_{ID_1}} \times \frac{e^{-\phi\mathcal{B}_2}e^{-\Theta_1\Theta_2}}{(\phi\mathcal{B}_1)^{n+1}}\sum_{j=0}^{n}\binom{n}{j}(-\Theta_2)^{n-j}\left[(-1)^{n-j+1}\Theta_1^{n-j} \times \frac{\text{Ei}(\Theta_1\Theta_2)}{(n-j)!} + \frac{e^{-\Theta_1\Theta_2}}{\Theta_2^{n-j}}\sum_{k=0}^{n-j-1}\frac{(-1)^k(\Theta_1\Theta_2)^k k!}{(n-j-k)!}\right], \tag{17}$$

where $\Theta_1 = \frac{1}{\phi\mathcal{B}_1\lambda_{ID_1}}$, $\Theta_2 = \frac{1}{\lambda_{SI}}$, and $\text{Ei}(\cdot)$ is the exponential integral function [12, eq. 8.211].

Proof: See Appendix A. ∎

By following the same steps of derivation used to compute (17) in Appendix A, and by making use of [15, eq. 9.6.7] and the approximation $e^{-x} \simeq 1 - x$ for small x, we derive the asymptotic expression for $P_{D_1}^{\text{out},t_2}$ in the high-SNR regime as

$$P_{D_1,asy}^{\text{out},t_2} = \phi e^{-K}\left(\frac{\gamma_{D_1}^{\text{th}}}{\alpha_1^*\rho_s} + \frac{1}{\lambda_{SI}\lambda_{ID_1}}\right). \tag{18}$$

2) Far-User D_2: The outage event for D_2 takes place either when the IoT-transmitter node I is unable to decode the symbol x_2 or when the node D_2 is unable to detect any symbol in conjunction with the successful detection of x_2 at node I. Hence, the OP expression for D_2 can be given as

$$P_{D_2}^{\text{out},t_2} = \Pr\left[\gamma_{S\to I}^{x_2,t_1} < \gamma_{D_2}^{\text{th}}] + \Pr[\gamma_{S\to I}^{x_2,t_1} \ge \gamma_{D_2}^{\text{th}}, \overline{P}_{SD_2}\right], \tag{19}$$

where $\overline{P}_{SD_2}$ signifies the probability of failure to detect any symbol at D_2 and can be given as

$$\overline{P}_{SD_2} = 1 - \Pr\left[\gamma_{I\to D_2}^{x_i,t_2} > \gamma_R^{\text{th}}, \gamma_{I\to D_2}^{x_2,t_2} > \gamma_{D_2}^{\text{th}}\right], \tag{20}$$

with $\gamma_R^{\text{th}} = 2^{2r_r} - 1$. After substituting the respective SINRs in (20) and with some mathematical re-arrangement, we get

$$\overline{P}_{SD_2} = 1 - \Pr\left[|h_{ID_2}|^2 > \frac{\max\{\mathcal{A}_3, \mathcal{A}_4\}}{|h_{SI}|^2\rho_s}\right] = \Pr\left[Y \le \frac{\Delta_2}{X\rho_s}\right], \tag{21}$$

where $\Delta_2 \triangleq \max\{\mathcal{A}_3, \mathcal{A}_4\}$, $\mathcal{A}_3 = \frac{\gamma_R^{\text{th}}}{(\alpha_4 - \psi_2\alpha_3\gamma_R^{\text{th}})\beta\mu}$, $\mathcal{A}_4 = \frac{\gamma_{D_2}^{\text{th}}}{(\alpha_3 - \alpha_4\gamma_{D_2}^{\text{th}})\beta\mu}$, and $Y \triangleq |h_{ID_2}|^2$ with condition $\frac{\alpha_4}{\psi_2\alpha_3} > \gamma_R^{\text{th}}$ and $\frac{\alpha_3}{\alpha_4} > \gamma_{D_2}^{\text{th}}$. One can deduce a permissible range of PAF from these imposed constraints to maintain the quality of service for the primary users as $\frac{\gamma_{D_2}^{\text{th}}}{1+\gamma_{D_2}^{\text{th}}} < \alpha_3 < \frac{1}{1+\psi_2\gamma_R^{\text{th}}}$. By inserting (21) into (19), one can derive the expression for $P_{D_2}^{\text{out},t_2}$ as given in the following theorem.

Theorem 2: The analytical expression for $P_{D_2}^{\text{out},t_2}$, conditioned over $\frac{\alpha_2}{\alpha_1} > \gamma_{D_2}^{\text{th}}$, can be given by

$$P_{D_2}^{\text{out},t_2} = 1 - \sum_{l=0}^{\infty}\frac{(-1)^l}{l!}\left(\frac{\Delta_2}{\lambda_{ID_2}\rho_s}\right)^l\frac{1}{\lambda_{SI}}\left(\frac{\mathcal{A}_5}{\rho_s}\right)^{1-l}\text{E}_l\left(\frac{\mathcal{A}_5}{\lambda_{SI}\rho_s}\right), \tag{22}$$

where $\mathcal{A}_5 = \frac{\gamma_{D_2}^{\text{th}}}{(\alpha_2 - \alpha_1\gamma_{D_2}^{\text{th}})(1-\beta)}$ and $\text{E}_l(\cdot)$ is the l-th order exponential integral function [15, eq. 5.1.1].

Proof: See Appendix B. ∎

Furthermore, with the use of approximation $e^{-x} \simeq 1 - x$ for small x and following the similar steps used to derive (22) in Appendix (B), the asymptotic expression for $P_{D_2}^{\text{out},t_2}$ at high SNR can be obtained as

$$P_{D_2,asy}^{\text{out},t_2} = \frac{\mathcal{A}_5}{\lambda_{SI}\rho_s} - \left(\frac{\Delta_2}{\lambda_{ID_2}\lambda_{SI}\rho_s}\right)\text{Ei}\left(-\frac{\mathcal{A}_5}{\lambda_{SI}\rho_s}\right). \tag{23}$$

3) IoT-Receiver R: The OP for R can be formulated as

$$P_R^{\text{out},t_2} = \Pr\left[\gamma_{S\to I}^{x_2,t_1} < \gamma_{D_2}^{\text{th}}] + \Pr[\gamma_{S\to I}^{x_2,t_1} \ge \gamma_{D_2}^{\text{th}}, \gamma_{I\to R}^{x_i,t_2} < \gamma_R^{\text{th}}\right]. \tag{24}$$

By invoking the respective SINRs in (24) with some algebraic manipulations, P_R^{out,t_2} can be expressed as

$$P_R^{\text{out},t_2} = \Pr\left[X < \frac{\mathcal{A}_5}{\rho_s}\right] + \Pr\left[X \ge \frac{\mathcal{A}_5}{\rho_s}, Z \le \frac{\mathcal{A}_6}{X\rho_s}\right], \tag{25}$$

where $Z \triangleq |h_{IR}|^2$ and $\mathcal{A}_6 = \frac{\gamma_R^{\text{th}}}{(\alpha_3 - \alpha_4\gamma_R^{\text{th}})\beta\mu}$. The analytical expression for P_R^{out,t_2} in (25), under the conditions $\frac{\alpha_2}{\alpha_1} > \gamma_{D_2}^{\text{th}}$ and $\frac{\alpha_3}{\alpha_4} > \gamma_R^{\text{th}}$, can be derived as given in the subsequent theorem.

Theorem 3: The analytical expression for P_R^{out,t_2} derived over Rayleigh fading channel can be given by

$$P_R^{\text{out},t_2} = 1 - \sum_{l=0}^{\infty}\frac{(-1)^l}{l!}\left(\frac{\mathcal{A}_6}{\lambda_{IR}\rho_s}\right)^l\frac{1}{\lambda_{SI}}\left(\frac{\mathcal{A}_5}{\rho_s}\right)^{1-l}\text{E}_l\left(\frac{\mathcal{A}_5}{\lambda_{SI}\rho_s}\right). \tag{26}$$

Proof: By following the similar steps used to obtain (22) in Appendix (B), one can derive (26). ∎

By following the analogous steps used to derive (23), one can obtain the asymptotic expression for P_R^{out,t_2} at high SNR as

$$P_{R,asy}^{\text{out},t_2} = \frac{\mathcal{A}_5}{\lambda_{SI}\rho_s} - \left(\frac{\mathcal{A}_6}{\lambda_{IR}\lambda_{SI}\rho_s}\right)\text{Ei}\left(-\frac{\mathcal{A}_5}{\lambda_{SI}\rho_s}\right). \tag{27}$$

Remarks: Despite the fact that final OP expressions in (17), (22), and (26) contain an infinite series, the numerical results elucidate that it converges to the exact solution with the first 40 terms. Moreover, using the definition of the diversity gain, the asymptotic OP expressions in (14) and (18) imply that the diversity order of

D_1 is one in the first phase and zero in the second phase (this can be explained intuitively by the fact that D_1 faces interference from the secondary transmission during the second phase). As for the asymptotic OP expressions in (23) and (27), with the aid of the following approximation $\mathrm{Ei}(x) \approx C + \ln(-x) + x$ for small x (where C is the Euler's constant), it can be inferred that the diversity order is one for both D_2 and R.

B. System Throughput

For a relay based wireless network, the system throughput is a measure of the average SE. The system throughput for the proposed EH-based CDRT-NOMA system is evaluated as the total of individual target rates for both primary and secondary communications that can be attained successfully over Rician/Rayleigh fading channels. It can be formulated as

$$\mathcal{S}_{\mathcal{T}} = \frac{1}{2}\left[\left(1 - P_{D_1}^{\text{out},t_1}\right) r_{d_1} + \left(1 - P_{D_1}^{\text{out},t_2}\right) r_{d_1} + \left(1 - P_{D_2}^{\text{out},t_2}\right) r_{d_2} + \left(1 - P_{R}^{\text{out},t_2}\right) r_r\right]. \quad (28)$$

C. Energy Efficiency

The EE is measured as the ratio of total data delivered to the total power consumed by the proposed system. It can be given by $\Xi_{\mathcal{E}} = \frac{\mathcal{S}_{\mathcal{T}}}{P_s/2}$, where $\mathcal{S}_{\mathcal{T}}$ is the achievable throughput as expressed in (28).

IV. Deep Learning Architecture

Here, we develop a DNN model to predict the OP and ESC of the system. As the conventional approaches and Monte-Carlo simulations to calculate the OP and ESC are intractable and cumbersome, respectively, this DNN model will help to predict OP and ESC in a short time and with less computational complexity.

A. Description of DNN Model

The proposed DNN model consists of training and prediction phases. In the training phase, the model is trained to learn the input-output relationship of the proposed CDRT-NOMA system using an adaptive moment estimation optimization algorithm in order to lower the loss function during a back-propagation operation offline. The trained DNN model is used for the online estimation of the OP/ESC value whenever a new data set is available at the input of the DL model in the prediction phase. As the training phase takes place offline, the network design can lower computational complexity and execution time.

The proposed DNN model has one input layer, multiple hidden layers, and one output layer. The input layer has nine neurons with nine parameters (i.e., $P_s, \beta, \alpha_1, \alpha_3, \psi_1, \psi_2, r_{d_1}, r_{d_2}, r_r$). There are four hidden layers, each with 100 neurons with an exponential linear unit (ELU) as the activation function. The output layer comprises one neuron that exploits the linear activation to compute the predicted value.

B. Dataset Generation

The following set of parameters have been taken as input for the proposed DNN model: source power $P_s \in [0, 40]$ dB, PS factor $\beta \in [0.01, 0.99]$, dual PAFs $\alpha_1 \in [0, 0.49]$ and $\alpha_3 \in [0.5, 0.99]$, the corresponding residual interference coefficients $\psi_1 \in [0, 0.1]$ and $\psi_2 \in [0, 0.1]$, and the target data rates $r_{d_1} \in [0.25, 1]$, $r_{d_2} \in [0.25, 0.8]$, and $r_r \in [0.25, 0.8]$. From these setups, we generate a dataset with 120,000 samples i.e., ($\mathcal{V} = 120,000$), where 80% is used for training, and the remaining 20% is used for validation and testing. To check the performance of the proposed DNN model, we use the root mean squared error (RMSE) to determine the difference between the natural OP/ESC values and the predicted ones across the entire test set. The data set generation is solely accountable for the complexity of the proposed model, while the number of floating-point operations determines the computational cost incurred during the prediction process. Our model has a computation cost of 31,101 trainable parameters.

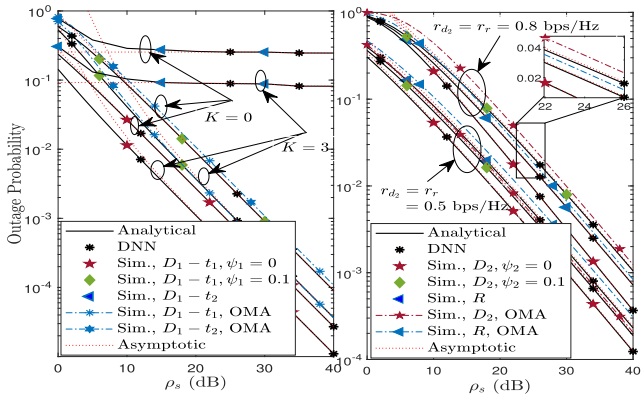

Fig. 2. OP of D_1, D_2 and R versus SNR.

V. Numerical Results

This section presents the numerical findings illustrating the performance of the proposed system. The analytical results are verified by Monte-Carlo simulations. We have also included the DNN model results here. The following set of parameters [6] is used throughout this section, unless stated otherwise [10]: $\alpha_1 = 0.3$, $\alpha_3 = 0.8$, $\alpha_1^* = 1$, $\beta = 0.3$, $\mu = 0.7$, and $\sigma^2 = 1$. Considering the 2-dimensional (x, y) plane, the positions for nodes S, D_1, I, D_2, and R are given as $(0, 0)$, $(0, -0.3)$, $(0.4, 0)$, $(0.5, 0)$, and $(-0.2, -0.45)$, respectively.

Fig. 2 depicts the OP performance versus the transmit SNR (ρ_s) for D_1, D_2, and R under the pSIC and ipSIC cases. Herein, we set the parameters as $r_{d_1} = 1$ bps/Hz, $r_{d_2} = r_r = \{0.5, 0.8\}$ bps/Hz. It can be seen from the curves that our simulation results are well aligned with the analytical ones as well as the DNN predictions. For D_1, when we increase the Rician-K factor from 0 to 3, the OP performance improves. This is expected since the viability of the line-of-sight increases with K. For D_2 and R, as the target rate ($r_{d_2} = r_r$) increases from 0.5 to 0.8 bps/Hz, the outage performance degrades. It is also worth noting that when we increase the level of residual interference parameter, the performance of D_1 and D_2 deteriorates. It indicates that the decoding capability of D_1 and D_2 decreases with an increase in the ipSIC level. Furthermore, the OP of the proposed EH-based CDRT-NOMA system model is compared with the OMA equivalent, which clearly shows the superiority of the former over the latter. In addition, for all the users, the asymptotic curves attained from the derived expressions and the corresponding simulated ones overlap in high-SNR regions, which corroborates the proposed asymptotic analysis.

Fig. 3(a) depicts the EC versus transmit SNR (ρ_s) curves for D_1, D_2, and R under both the pSIC and ipSIC cases. We observe that as SNR increases, the EC of the system improves. The results demonstrate that the ESC of our proposed system achieves better performance in comparison to its OMA equivalent in the case of pSIC. In addition, it demonstrates that the simulation and DNN prediction results are highly congruent, validating our DL framework.

In Fig. 3(b), we plot the throughput of the proposed system as a function of ρ_s for both pSIC and ipSIC cases under the parameter settings $r_{d_1} = 1$ bps/Hz, $r_{d_2} = r_r = \{0.5, 0.8\}$ bps/Hz, $K = 3$, with different values of PS factor $\beta = 0.2, 0.5$. We can see that the system throughput increases from lower to medium range of the SNR, and subsequently gets saturated, reflecting the maximum

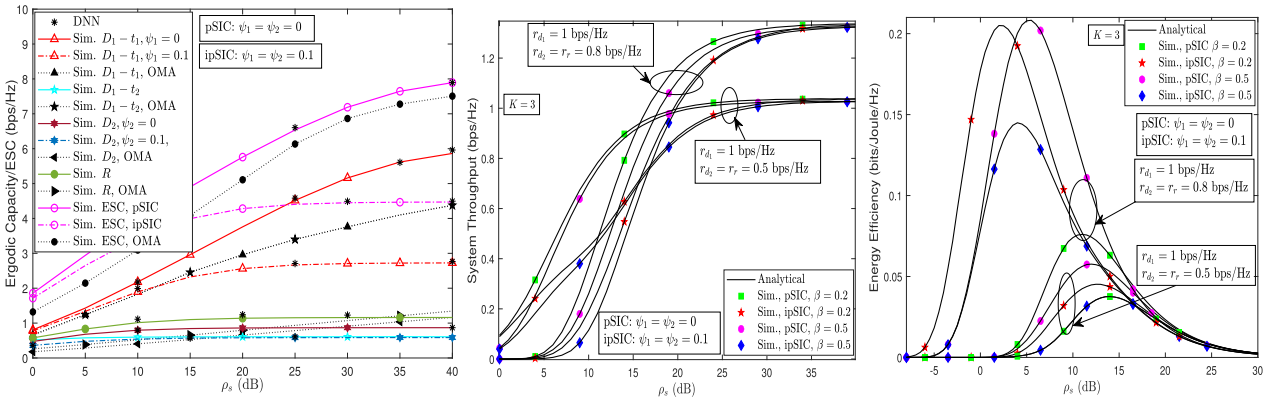

Fig. 3. (a) EC/ESC versus SNR; (b) System throughput versus SNR; (c) Energy efficiency versus SNR.

attainable throughput for the specific data rate. For the higher data rate, it attains its maximum at relatively high SNR. It happens because the outage performance at a higher target rate is relatively poorer than the lower target rate.

In Fig. 3(c), we plot the EE of the proposed system as a function of ρ_s for both pSIC and ipSIC cases with the same set of parameters as the ones used in Fig. 3(c). We observe that the EE first increases as ρ_s increases from low- to medium- SNR region. For higher SNR values, the EE of both pSIC and ipSIC starts to decay and to converge because of the higher power consumption of the network.

Moreover, we compare the execution time taken by the Monte-Carlo simulation and the DNN for ESC evaluation. It is noted that the DNN prediction takes 0.0175 seconds, compared to 4.95 seconds for the Monte-Carlo simulation. Also, the proposed DL framework has the lowest RMSE of 1.43×10^{-3}. One can observe hereby that the DL framework exhibits a low execution time as compared to the Monte-Carlo simulation to evaluate the ESC, which helps to explore real-time configurations for the proposed system.

APPENDIX A

We can evaluate $P_{D_1}^{\text{out},t_2}$ in (16) as

$$P_{D_1}^{\text{out},t_2} = \int_0^\infty \left(\int_0^\infty F_W(\mathcal{B}_1 xv + \mathcal{B}_2) f_X(x) dx \right) f_V(v) dv. \quad (29)$$

By substituting the CDF of W in infinite series form utilizing [12, eq. 8.445] and [13, eq. 4.35], (29) can be expressed as

$$P_{D_1}^{\text{out},t_2} = \int_0^\infty \left(\int_0^\infty \left(1 - \sum_{l=0}^{\infty} \sum_{m=0}^{l} \frac{K^l \phi^m e^{-K} (\mathcal{B}_1 xv + \mathcal{B}_2)^m}{l! m!} \times e^{-(\mathcal{B}_1 xv + \mathcal{B}_2)} \right) f_X(x) dx \right) f_V(v) dv. \quad (30)$$

By substituting the respective PDFs and utilizing the binomial expansion [12, eq. 1.111] and [12, eq. 3.351.1] to solve (29) rigourously, one can obtain the result as given in (17).

APPENDIX B

By substituting (6) and (21) in (19) and with some mathematical re-arrangement, $P_{D_2}^{\text{out},t_2}$ can be evaluated as

$$P_{D_2}^{\text{out},t_2} = \Pr\left[X < \frac{\mathcal{A}_5}{\rho_s} \right] + \Pr\left[X \geq \frac{\mathcal{A}_5}{\rho_s}, Y \leq \frac{\Delta_2}{X \rho_s} \right] = 1 - \frac{1}{\lambda_{SI}} \int_{\frac{\mathcal{A}_5}{\rho_s}}^\infty e^{-\frac{\Delta_2}{\lambda_{ID_2} \rho_s x}} e^{-\frac{x}{\lambda_{SI}}} dx. \quad (31)$$

Since the integral in (31) is intractable, we utilize the Maclaurin series expansion for the term $e^{-\frac{\Delta_2}{\lambda_{ID_2} \rho_s x}}$ to simplify (31) as

$$P_{D_2}^{\text{out},t_2} = 1 - \sum_{l=0}^{\infty} \frac{(-1)^l}{l!} \left(\frac{\Delta_2}{\lambda_{ID_2} \rho_s} \right)^l \frac{1}{\lambda_{SI}} \int_{\frac{\mathcal{A}_5}{\rho_s}}^\infty \frac{e^{-\frac{x}{\lambda_{SI}}}}{x^l} dx. \quad (32)$$

By solving the integral term in (32), (22) can be obtained.

REFERENCES

[1] Y. Liu et al., "Cooperative non-orthogonal multiple access with simultaneous wireless information and power transfer," *IEEE J. Sel. Areas Commun.*, vol. 34, no. 4, pp. 938–953, Apr. 2016.

[2] Z. Ding et al., "Cooperative non-orthogonal multiple access in 5G systems," *IEEE Commun. Lett.*, vol. 19, no. 8, pp. 1462–1465, Aug. 2015.

[3] X. Yue et al., "Exploiting full/half-duplex user relaying in NOMA systems," *IEEE Trans. Commun.*, vol. 66, no. 2, pp. 560–575, Feb. 2018.

[4] J.-B. Kim and I.-H. Lee, "Non-orthogonal multiple access in coordinated direct and relay transmission," *IEEE Commun. Lett.*, vol. 19, no. 11, pp. 2037–2040, Nov. 2015.

[5] L. Zou et al., "Capacity enhancement of D2D aided coordinated direct and relay transmission using NOMA," *IEEE Commun. Lett.*, vol. 24, no. 10, pp. 2128–2132, Oct. 2020.

[6] T.-T. Nguyen et al., "IoT-based coordinated direct and relay transmission with non-orthogonal multiple access," *IEEE Wireless Commun. Lett.*, vol. 10, no. 3, pp. 503–507, Mar. 2021.

[7] A. Jee et al., "A coordinated direct AF/DF relay-aided NOMA framework for low outage," *IEEE Trans. Commun.*, vol. 70, no. 3, pp. 1559–1579, Mar. 2022.

[8] T.-H. Vu et al., "Performance analysis and deep learning design of underlay cognitive NOMA-based CDRT networks with imperfect SIC and co-channel interference," *IEEE Trans. Commun.*, vol. 69, no. 12, pp. 8159–8174, Dec. 2021.

[9] M.-T. Nguyen et al., "Performance analysis of wireless powered cooperative NOMA-based CDRT IoT networks," *IEEE Syst. J.*, vol. 16, no. 4, pp. 6501–6512, Dec. 2022.

[10] A. K. Shukla et al., "Exploiting SWIPT-enabled IoT-based cognitive nonorthogonal multiple access with coordinated direct and relay transmission," *IEEE Sensors J.*, vol. 22, no. 19, pp. 18988–18999, Oct. 2022.

[11] D. Wan et al., "Cooperative NOMA systems with partial channel state information over Nakagami-m fading channels," *IEEE Trans. Commun.*, vol. 66, no. 3, pp. 947–958, Mar. 2018.

[12] I. S. Gradshteyn and I. M. Ryzhik, *Tables of Integrals, Series and Products*, 6th ed. New York, NY, USA: Academic, 2000.

[13] M. K. Simon and M.-S. Alouini, *Digital Communication Over Fading Channels: A Unified Approach to Performance Analysis*. New York, NY, USA: Wiley, 2000.

[14] L. Liu et al., "Wireless information and power transfer: A dynamic power splitting approach," *IEEE Trans. Commun.*, vol. 61, no. 9, pp. 3990–4001, Sep. 2013.

[15] M. Abramowitz and I. A. Stegun, *Handbook of Mathematical Functions With Formulas, Graphs, and Mathematical Tables* (NBS Applied Mathematics Series 55). New York, NY, USA: National Bureau of Standards, 1972.